Characterization of STARDUST target comet 81P/Wild 2 from 1996 to 1998

Schulz, R.; Stüwe, J.A.; Boehnhardt, H.; Gaessler, W.; Tozzi, G.P.

A&A 398, 345–352 (2003)
DOI: 10.1051/0004-6361:20021673

Astronomy & Astrophysics

Characterization of STARDUST target comet 81P/Wild 2 from 1996 to 1998⋆

R. Schulz[1], J. A. Stüwe[2], H. Boehnhardt[3], W. Gaessler[4], and G. P. Tozzi[5]

[1] Research and Scientific Support Department of ESA, ESTEC, Postbus 299, 2200 AC Noordwijk, The Netherlands
e-mail: Rita.Schulz@esa.int
[2] Sterrewacht Leiden, Postbus 9513, 2300 RA Leiden, The Netherlands
e-mail: stuwe@strw.leidenuniv.nl
[3] European Southern Observatory Chile, Alonso de Cordova 3107, Santiago, Vitacura, Chile
e-mail: hboehnh@eso.org
[4] Subaru Telescope, National Astronomical Observatory of Japan, 650 North A'ohoku Place, Hilo, HI 96720, USA
e-mail: Wolfgang.Gaessler@SubaruTelescope.org
[5] Osservatorio Astrophisico di Arcetri, Largo E. Fermi 5, 50125 Firenze, Italy
e-mail: tozzi@arcetri.astro.it

Received 11 March 2002 / Accepted 5 November 2002

Abstract. We present the results of our monitoring of comet 81P/Wild 2, the target of the STARDUST mission. Broad-band filter images and medium resolution spectra of this comet obtained along its pre- and postperihelion orbit between 1996 and 1998 were analysed in terms of coma morphology and activity. The morphological coma investigation revealed the presence of long-lasting fan structures, which remained essentially unchanged for at least three months. The $(B-V)$ and $(V-R)$ colour indices were determined at three different positions along the orbit. The two-dimensional analysis showed a uniform colour over the entire coma. Hence, the material composing the structures is not different from that of the underlying coma. The distribution of coma brightness as a function of projected distance from the nucleus shows no peculiarities. The evolution of the comet's activity during the pre- and postperihelion phase appears to be asymmetric in that activity increases faster preperihelion than it decreases postperihelion. The production rates (or their upper limits in the case on a non-detection) of CN, C_2, C_3, and NH_2 were determined from the spectrophotometric observations and compared to other values published in the literature.

Key words. comets: general – comets: individual: 81P/Wild 2

1. Introduction

The perihelion passage of Comet 81P/Wild 2 on May 6, 1997 was the last one before the comet is visited by NASA's STARDUST space probe in January 2004. During a post-perihelion fly-by at r_h = 1.86 AU, STARDUST will obtain coma and nucleus images, monitor the cometary dust flux and analyse the composition of these particles in-situ, and collect coma material on a special capture medium (aerogel) for return to Earth (Brownlee et al. 1994). In order to guarantee a successful data and sample acquisition while minimizing the hazards to the spacecraft, some basic parameters of the target comet, particularly its coma, should be known before the encounter. The extensive characterization of a space mission target by remote-sensing techniques is, however, also essential for the advance of cometary science in general. To optimize the return of the STARDUST mission the results of the laboratory analysis of the returned sample and of the in-situ measurements (both obtained at a certain part of the orbit of comet 81P/Wild 2) should be put into the larger framework of the evolution of the comet along its orbit and its behaviour during other apparitions. Comet 81P/Wild 2 was recently deflected from a region in the outer Solar System between Jupiter and Uranus into its present Jupiter-family type orbit when it had a very close approach to Jupiter in 1974 (Marsden 1978). It is therefore generally regarded as a relatively fresh comet. From the observed depletion of the C_2 production rate (as compared to CN) at r_h = 2.33 AU, 81P/Wild 2 (like other C_2-depleted Jupiter-family comets) is suspected to originate from the Kuiper Belt rather than the Oort Cloud (A'Hearn et al. 1995). In this paper, we present the results of our pre- and postperihelion monitoring of the coma activity and morphology of comet 81P/Wild 2 during its last apparition and their relevance for the STARDUST encounter.

2. Observations and basic data reduction

Comet 81P/Wild 2 was observed from the European Southern Observatory, La Silla, Chile, at four different positions along its orbit. Altogether 16 broad-band filter images and 2 long-slit

Send offprint requests to: R. Schulz, e-mail: Rita.Schulz@esa.int
⋆ based on observations obtained at ESO La Silla within ESO programmes No. 57.F-0290, 58.F-0413, 58.F-0431 and 60.F-0266.

Table 1. Observations of comet 81P/Wild 2, the comet passed through its perihelion on May 6, 1997, 15:04 UT.

Date	UT	Telescope	Instrument	Filter Grism	Band	τ_{exp} s	Airmass AU	Δ AU	r_h	PA_{sun}	Phase
1996											
Sep 10[a)]	09:34	ESO 2.2m	EFOSC2	F.# 585	*R*	600	2.109	2.858	2.649	93.°2	20.°6
Sep 11	09:41	ESO 2.2m	EFOSC2	F.# 585	*R*	600	1.994	2.840	2.644	93.°4	20.°8
Dec 11	06:15	ESO 2.2m	EFOSC2	F.# 585	*R*	300	1.566	1.289	2.108	106.°2	19.°1
Dec 11	06:24	ESO 2.2m	EFOSC2	F.# 584	*V*	300	1.536	1.288	2.108	106.°2	19.°1
1997											
Apr 02	01:10	Dan 1.5m	DFOSC	F.# 452	*R*	180	1.646	0.992	1.620	283.°5	35.°7
Apr 02	01:26	Dan 1.5m	DFOSC	F.# 452	*R*	180	1.687	0.992	1.620	283.°5	35.°7
Apr 02	01:32	Dan 1.5m	DFOSC	F.# 451	*V*	360	1.714	0.992	1.620	283.°5	35.°7
Apr 02	01:44	Dan 1.5m	DFOSC	F.# 450	*B*	800	1.772	0.992	1.620	283.°5	35.°7
Apr 02	02:01	Dan 1.5m	DFOSC	F.# 452	*R*	180	1.828	0.992	1.620	283.°5	35.°7
Apr 03	01:08	Dan 1.5m	DFOSC	F.# 452	*R*	180	1.645	0.997	1.618	283.°6	35.°9
Apr 03	01:33	Dan 1.5m	DFOSC	Gr. # 4	*n/a*	900	1.739	0.997	1.618	283.°6	35.°9
Apr 03[b)]	02:20	Dan 1.5m	DFOSC	F.# 452	*R*	180	1.960	0.997	1.618	283.°6	36.°0
Apr 03[b)]	02:25	Dan 1.5m	DFOSC	F.# 451	*V*	180	1.996	0.997	1.618	283.°6	36.°0
Apr 03[b)]	02:30	Dan 1.5m	DFOSC	F.# 450	*B*	180	2.039	0.997	1.618	283.°6	36.°0
1998											
Mar 31	09:20	ESO 3.6m	EFOSC2	F.# 642	*R*	120	1.561	3.517	3.162	75.°4	16.°1
Mar 31	09:26	ESO 3.6m	EFOSC2	F.# 641	*V*	300	1.513	3.517	3.162	75.°4	16.°1
Mar 31	09:34	ESO 3.6m	EFOSC2	F.# 639	*B*	300	1.460	3.517	3.162	75.°4	16.°1
Mar 31	09:42	ESO 3.6m	EFOSC2	Gr. # 1	*n/a*	1200	1.378	3.517	3.162	75.°4	16.°1

[a)] Background star at nucleus position.
[b)] Background galaxy close to comet position.

low-resolution spectra were obtained between September 1996 and March 1998 (Table 1). The spectra cover the wavelength range 3400 Å with a resolution of 25 Å. A coarse description of the used broad-band filters is given in Table 2. For the precise specifications we refer to the *ESO Image Quality Filters Catalogue*. The specifics on the instruments may be obtained from the appropriate manuals (Melnick & Mendez de Oliveira, 1995 for the EFOSC2 at the ESO/MPG 2.2 m telescope; Patat, 1999 for the EFOSC2 at the ESO 3.6 m telescope and Brewer & Storm, 2001 for the DFOSC instrument at the Danish 1.54 m telescope). All observations were carried out under photometric conditions.

All reduction processes were done with the aid of ESO's Munich Image Data Analysis System, MIDAS (1998). We performed bias subtraction and flatfielding on all frames. To facilitate a calibration of the broad-band images, appropriate fields from the list of Landolt (1992) were observed at different airmasses each night. Reduction procedures of the ESO-MIDAS context "long" were applied to the spectrum frames, where the wavelength calibration of the spectra was done via HeAr- (EFOSC2) and HeNe-arc frames (DFOSC), respectively. Because of the long slit of the EFOSC2 (5′) as well as the DFOSC (13.′7) instruments the sky contamination in the spectra could be determined from the spectrum frames themselves. The extinction correction was performed assuming the standard atmospheric conditions described by Tüg (1977). For the flux calibration observations of the spectrophotometric standards LTT 3864, LTT 6248 & LTT 7987 taken on the same night were used.

3. Results

3.1. Coma morphology

The coma images were searched for the presence of distinct features. Such features correspond to local variations of the gradient in the two-dimensional intensity profile representing the undisturbed coma (cf. Schulz 1991). As these variations usually amount only a few percent of the whole dynamical range of the image, they only become visible after the smooth general intensity profile on which they are superimposed has been removed. This can be done by empirically fitting a smooth two-dimensional profile to the observed coma isophotes which is then subtracted from the orginal image. This technique effectively removes the underlying coma profile, hence enhances superimposed structures. The coma isophotes of comet 81P/Wild 2 were best represented by ellipses. Hence we applied an ellipse fitting scheme from the MIDAS context "surfphot" to the images, which is based on formulas published by Bender & Möllenhoff (1987). Figures 1–3 show the observed coma images their ellipsoidal fits and the residuals remaining after subtracting the ellipsoidal fits from the real comae.

Table 2. Specification of filters (effective wavelength, $\lambda_{\rm eff}$, and band width, $FWHM$) and grisms (blaze wavelength, $\lambda_{\rm blaze}$ and covered wavelength range.

Filter#	Band	$\lambda_{\rm eff}$	FWHM
		nm	nm
450	*B*	433.57	102.29
451	*V*	544.80	116.31
452	*R*	648.87	164.70
584	*V*	547.60	113.20
585	*R*	643.10	165.40
639	*B*	440.00	94.50
641	*V*	547.60	113.20
642	*R*	643.10	165.40

Grism#	$\lambda_{\rm blaze}$	Range		
	nm	nm		nm
4	580	350	...	700
1	450	319	...	1094

Table 3. Scalelength, κ, position angle, PA and width of the features detected in the broad-band images of 81P/Wild 2, together with the projected tail-direction, Tail, in parenthesis.

Date	Fan	κ	PA	Width
		10^4 km		
11.09.1996	I	5 ± 2	189°	90°
	Tail		(273°)	
	II	8 ± 3	358°	90°
11.12.1996	I	5 ± 2	190°	100°
	II	12 ± 2	283°	15°
	Tail		(286°)	
	III	2.1 ± 0.1	390° ... 340°	80°
02.04.1997	I	5.2 ± 0.4	10° ... 65°	40°
	II	5.3 ± 0.3	105°	30°
	Tail		(104°)	
	III	3.6 ± 0.3	240° ... 280°	70°
01.03.1998	n/a	*n/a*	*n/a*	*n/a*
	Tail		(255°)	

Several distinct features can clearly be identified. The structurally enhanced images of December 11, 1996, are dominated by a strong fan (i.e. >20% above the general brightness) which lies almost perpendicular to the sun-tail direction. The fan appears to be present already on September 11, 1996, although the signal-to-noise ratio of this observation is only poor. In April 1997 three features can clearly be identified in all frames. Their brightness is, however, much lower than that of the fan of December 1996. It lies only about 5% above the general coma brightness. Some basic properties of the detected fans are given in Table 3. The parameters listed here result from Gaussian fits to azimutal cuts through the respective fan at several nucleus distances. The numbering was arbitrarily chosen to coinside with the increasing position angle. The parameter κ is the scale-length of the feature computed from a $\ln Flux$ vs. ρ fit, whereby Flux represents the fitted Gaussian's central flux value and ρ stands for the nucleus distance. The listed position angle, PA, gives the center position of the Gaussian fit to the azimutal profile. The given width represents the computed $FWHM$. Whenever a range of position angles is listed, it gives the values covered between nucleus distances of 10 000 km to about 100 000 km. The calculated position angle of the anti-solar direction (Tail) is given in parenthesis. The exact values of the parameters presented in Table 3 are, of course, highly dependent on the applied enhancement technique. It is obvious, however, that all three features visible in April 1997 are already discernible (at similar positions with respect to the tail direction) in December 1996. However, at that time the brightness of the strongest feature is much higher than that of the other two. We suspect that the feature pointing into the projected tail direction represents the already developed dust tail, whereas the other two features seen in comet 81P/Wild 2 are long-lasting coma fans as first defined by Sekanina (1987) & further modelled by Sekanina & Boehnhardt (1997). The March 1998 observations show no evidence of distinct coma features. (The bright spot in the residual images of March 1998 is a background object.)

3.2. Coma profiles

For the analysis of the overall coma, one-dimensional profiles were obtained from the photometrically calibrated images. This is usually done by azimuthal averaging around the optocenter, which assumes the coma to be spherical symmetric. With the azimuthally averaged profiles the applicability of the fountain model to this comet may be investigated. For an ideal fountain model the coma brightness should vary with $\mu \sim 1/\rho$. In the double logarithmic representation the radial (azimuthally averaged) coma profiles should therefore be straight lines with a slope of $m = -1$. Jewitt and Meech (1987) showed that the limiting case of a steady-state coma profile distorted by solar radiation pressure is represented by a slope of $m = -1.5$. Figure 4 shows the coma profiles derived for comet 81P/Wild 2 together with the straight lines fitted to them. Each profile can reasonably well be represented by a straight line. The flattening of some profiles in the innermost coma ($\rho \leq 2500$ km) is artificial, because the profiles are oversampled here owing to the fact that the pixel size was significantly smaller than the seeing disk of typically 1″. In the outer coma (typically above $\rho = 20\,000$ km) the low signal-to-noise leads to a large uncertainty in the determination of the sky background, which most probably causes the deviations of the profiles from straight lines in this region. Profiles obtained in different filters on the same date show similar slopes (see Table 4). There appears to be a trend towards flatter profiles with decreasing heliocentric distance which may be explained by the increasing fraction of gaseous emissions (CN, C_2 and C_3) in the broad-band filters. On September 11, 1996, the coma profile exhibits an unusually high slope, which

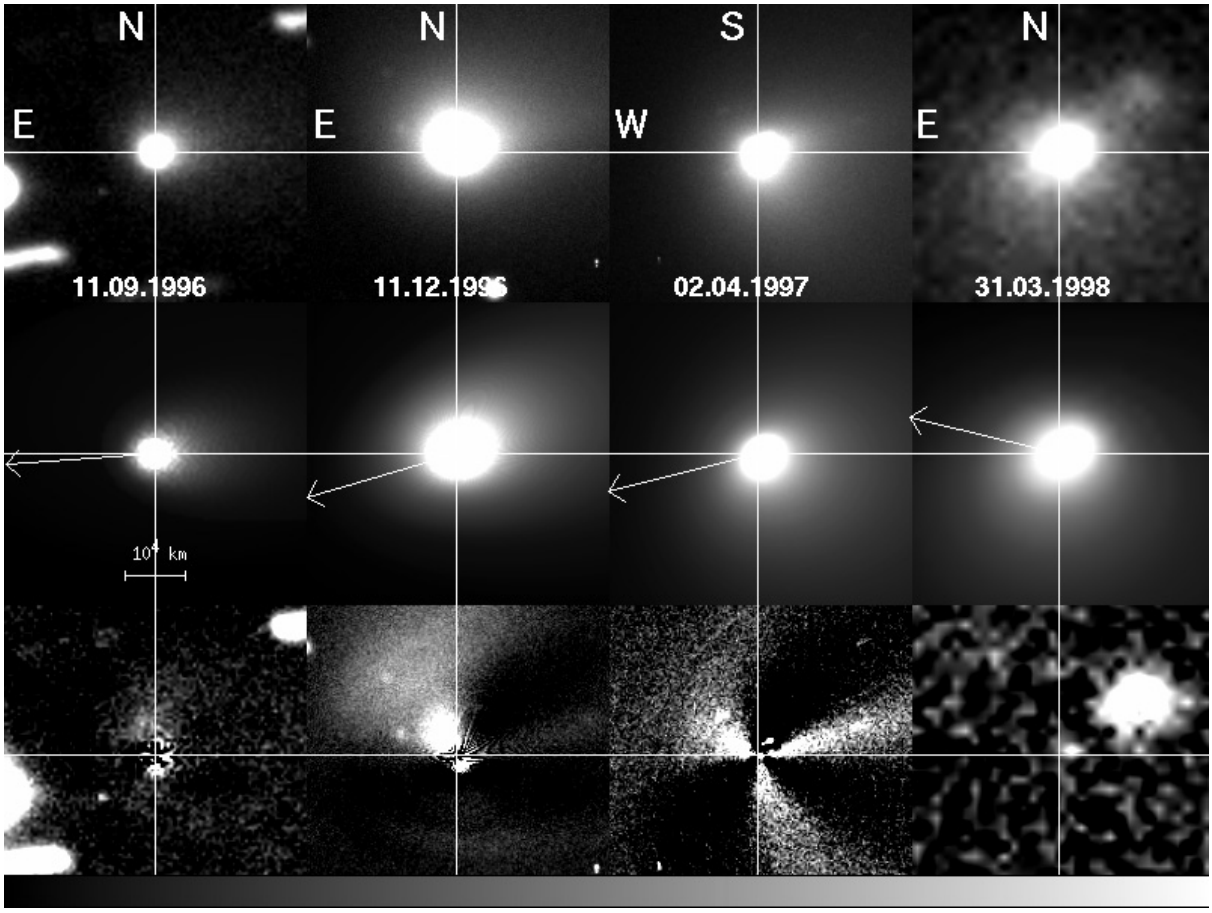

Fig. 1. Subtraction of an elliptical isophote fit from the broad-band *R* images. Upper panel: original image, middle panel: ellipse fit, lower panel: residual flux after subtraction of middle from upper panel image. The upper and middle panel gray scales are identical, whereas the lower panel is scaled to show deviations >20% for the 11.12.1996 and >5% for the other two dates. The arrows in the middle panel show the direction towards the sun.

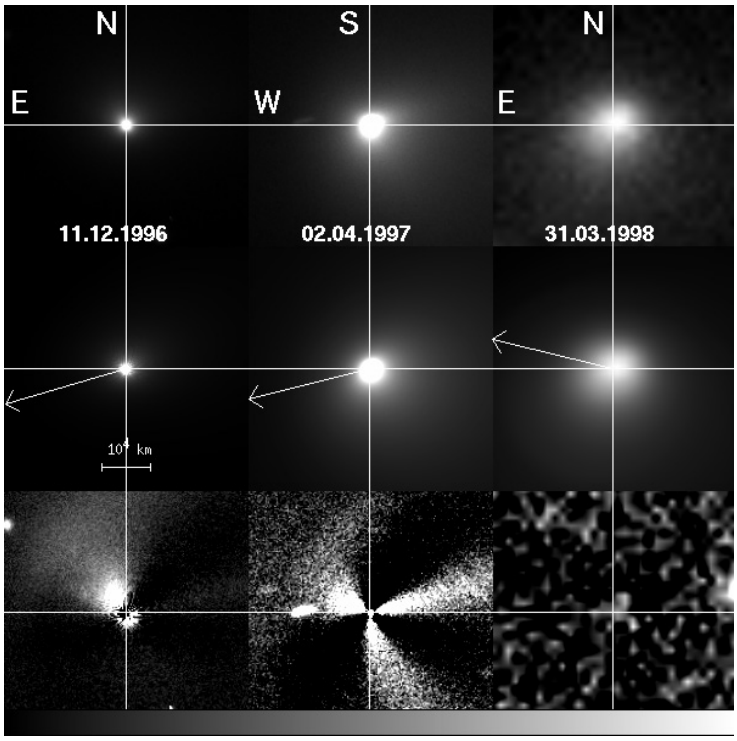

Fig. 2. Same as Fig. 1 for broad-band *V*.

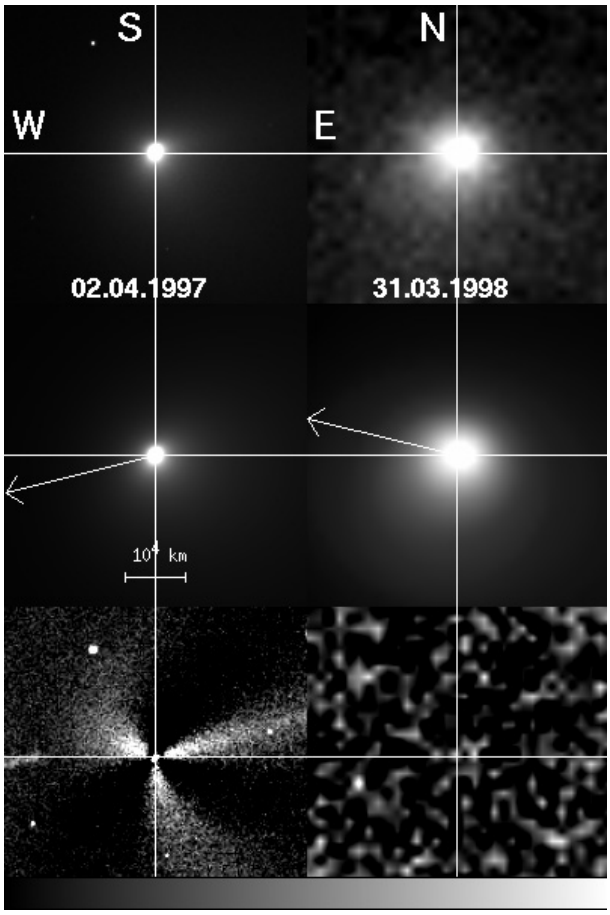

Fig. 3. Same as Fig. 1 for broad-band *B*.

cannot be explained by radiation pressure effects. However, we caution that this observation had to be taken in morning twilight at an airmass of about 2. The slopes of all other profiles are >-1.5, hence within the limits for a steady-state coma distorted by solar radiation pressure. The values of December 1996 and April 1997 are consistent with those resulting from similar observations of this comet obtained between February and June 1997 (Fink et al. 1999).

3.3. Colour determination

The coma of comet 81P/Wild 2 was slightly redder than the Sun. Table 5 lists the measured colour indices and the reddening (in % per 1000 Å) derived from the spectra and the images. The colour indices were averaged over the innermost 10 000 km of the coma to avoid effects of the sky background. For the spectra the reddening was determined from the clean continuum regions as well as from the regions covered by the respective broad-band filters (after convolution of the spectrum with the filter) using $R = F_{\mathrm{cont}(\lambda)}/F_{\mathrm{sun}(\lambda)} \times F_{V-\mathrm{band(sun)}}/F_{V-\mathrm{band(cont)}}$. For the images the fluxes in the *B* and *R* filters were used. Assuming an error of 10% in our measured flux values and of 3% in the tabulated values for the Sun, the values for the reddening show, within the margin of error, no significant differences between the spectra and the images. The $(V-R)$ colour indices do not differ much over the entire

Table 4. The slopes of the straight lines fitted to the profiles of Fig. 4.

Date	*R*	*V*	*B*
11.09.1996	−1.85	-	-
11.12.1996	−1.37	−1.34	-
02.04.1997	−1.20	−1.14	− − 1.12
31.03.1998	−1.37	−1.45	−1.43

data set, however, the $(B-V)$ value of 1997 indicates a significantly bluer coma than in 1998. This is a direct result of the gaseous emission present in 1997. The rather weak C_2 emission bands are covered by both, the broad-band *R* and the broad-band *V* filters (see Table 2) whereas the C_3 and CN emissions, in particular the strong CN (0-0) band, contribute only to the broad-band *B* filter.

Comet 81P/Wild 2 had a uniform colour over the entire coma that could be investigated up to where the signal hit the sky background. Radial colour profiles, which could be analysed up to a radius of about 13 000 km, showed a constant value as a function of nucleus distance. Colour index images computed from the original frames do not show any distinct features. This means that there is no obvious difference between the material composing the structures and that of the general coma.

3.4. $Af\rho$

Since the *R* band-pass is roughly centered at $\lambda \approx 6400$ Å, with an equivalent width of $W_R \approx 1450$ Å, it should be least affected by possibly present gaseous emission, as the next strongest bands (i.e. those of C_3 & C_2) are located in the blue to green spectral range (see Fig. 5). In order to compute $Af\rho$ values from the magnitude calibrated *R* data, the values had to be converted to fluxes via the constants provided by Bessell et al. (1998). The also necessary solar flux values were computed by folding the solar spectrum as given by Colina et al. (1996) with the transmission curves of the actually used filters. Table 6 shows the $Af\rho$ values computed from the azimutally averaged coma profiles in the *R* filter (aperture radius: 10 000 km). They are in excellent agreement with those derived from the spectroscopic observations for the two nights both types of observations exist (see Table 7). The $Af\rho$ values indicate that the increase in dust production is much stronger during the preperihelion phase than its postperihelion decrease.

3.5. Spectra

After the basic reduction steps described in Sect. 2, the two spectra were analysed and searched for emission features. Both spectra are depicted in Fig. 5. Figure 6 shows them before continuum subtraction. The signal-to-noise ratio of the spectrum taken on March 31, 1998, is rather low, owing to the large distance of Comet 81P/Wild 2 at that time. Hence, no emission features are detectable. The spectrum of April 3, 1997, however, clearly shows emission bands of CN ($\lambda \approx 3870$ Å), C_3 ($\lambda \approx 4070$ Å), C_2 ($\lambda \approx 5100$ Å) and NH_2 ($\lambda \approx 5700$ Å).

Their production rates were determined from the fluxes

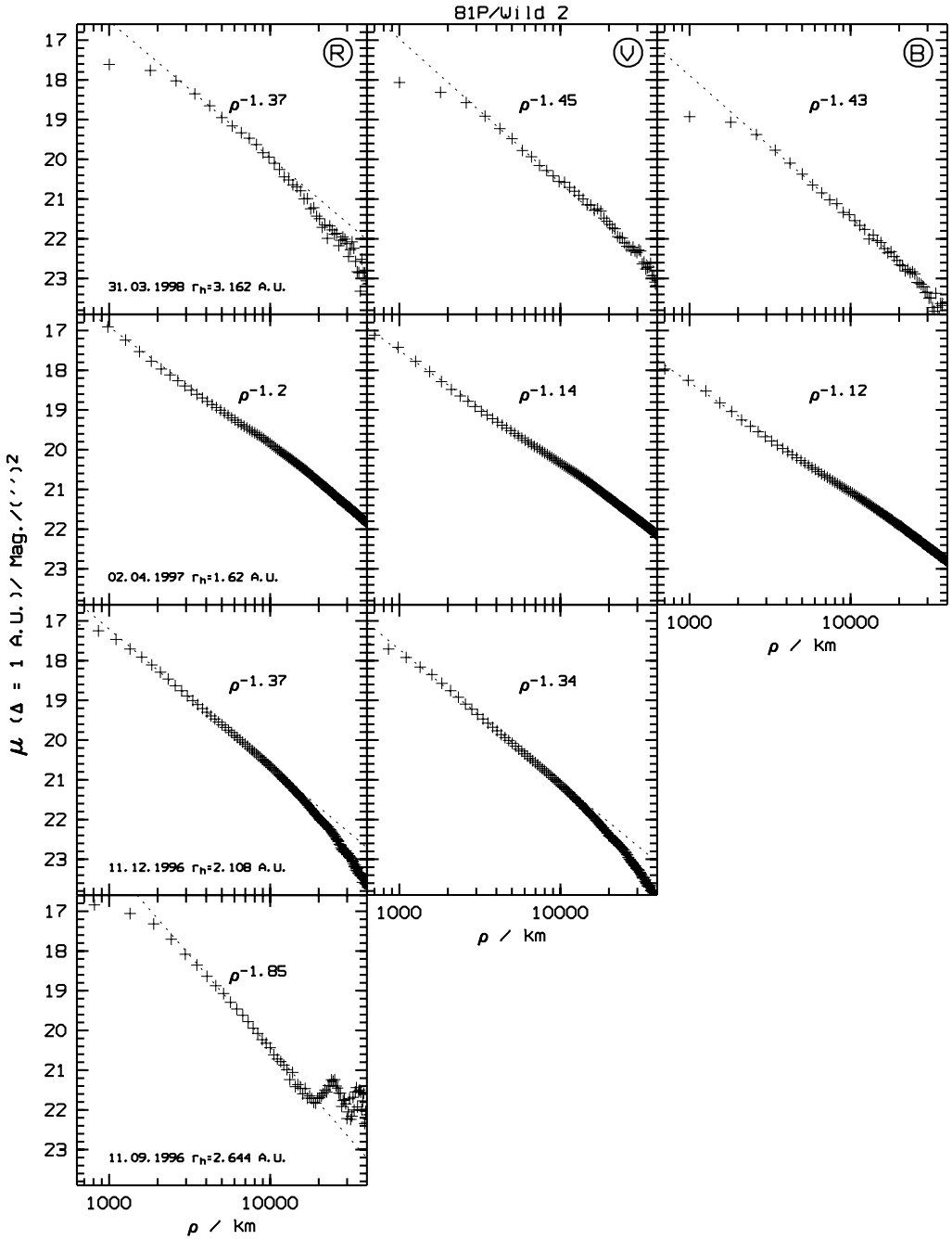

Fig. 4. Azimutally averaged broad-band surface brightness, μ, reduced to a geocentric distance of 1 AU, as a function of apparent nucleus distance, ρ. The dashed line indicates the result of a double logarithmic fit of: flux vs. $\rho^{-\beta}$. The columns show the profiles in *R*, *V* and *B* (from left to right).

integrated over the slit length corresponding to the entire detectable coma. For the continuum subtraction a reddened solar spectrum (Colina et al. 1996) was fitted to the data. For CN, C_3, and C_2 the fluxes were converted into column densities using the fluorescence efficiencies applied by A'Hearn et al. (1995), taking into account the dependences on heliocentric distance and radial velocitiy in the case of CN (Schleicher 1983). For NH_2 the g-factors published by Tegler & Wyckoff (1989) divided by a factor of 2 to account for the odd-even effect (Arpigny 1995) were used. These values vary from those determined by Kawakita et al. (2001) by a factor of 1.09 (April 1997) and 1.06 (March 1998). The production rates and upper limits given in Table 7 were calculated with the Vectorial model (Festou 1981) and the lifetimes given by Schulz et al. (1994; 1998). The parent velocity was varied as 0.85 km s^{-1} $\times$ $r^{-0.5}$ (Cochran & Barker 1986) while the daughter velocity was arbitrarily set to 1 km s^{-1}. The $Af\rho$ values in Table 7 were derived from the spectra by extracting a spatial profile of the flux emitted in the wavelength range 6400 Å $< \lambda <$ 6800 Å and computing $Af\rho$ according to A'Hearn et al. (1984). The effective aperture radius was 10 000 km. The solar flux in the quoted wavelength range (needed to compute values for $Af\rho$) was taken from Colina et al. (1996).

Table 5. Colour indices and the reddening of Comet 81P/Wild 2. $Red_{\rm ima}$: reddening derived from images. $Red_{\rm spec+fil}$: reddening derived from spectra convolved with respective filter curves. $Red_{\rm spec}$: reddening derived from regions of clean continuum in the spectra.

Date	$(B-V)$	$(V-R)$	$Red_{\rm ima}$	$Red_{\rm spec+fil}$	$Red_{\rm spec}$
	Mag.	Mag.	% /1000 Å	% /1000 Å	% /1000 Å
11.12.1996		0.47 ± 0.02	9.1		
02.04.1997	0.74 ± 0.01	0.51 ± 0.01	13.1 ± 3.0	12.0 ± 8.1	6.2 ± 5.0
31.03.1998	0.85 ± 0.03	0.57 ± 0.07	17.2 ± 2.0	52 ± 50	42 ± 35
Sun	0.649	0.37			

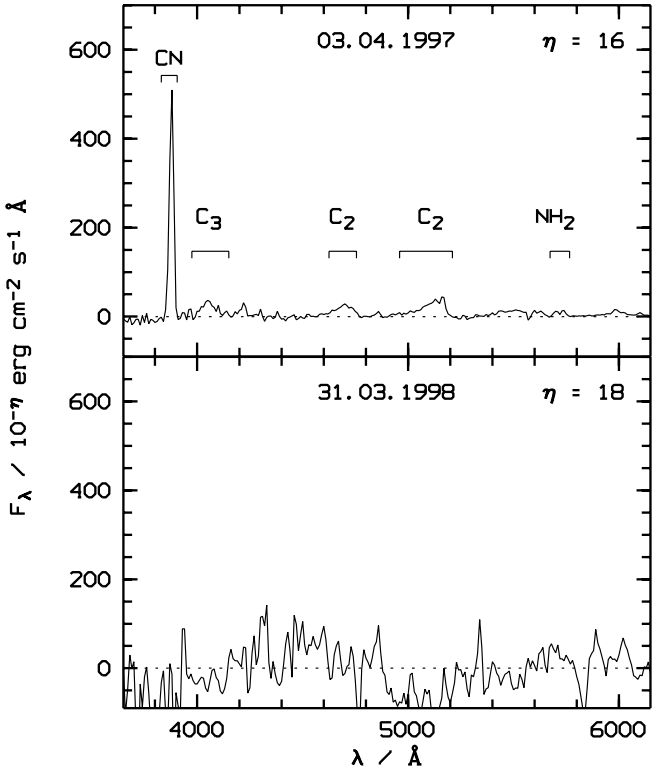

Fig. 5. Spectra of Comet 81P/Wild 2. A reddened solar analogue spectrum was subtracted from the data. Note the different exponent η in the flux units enhancing the flux scale in the 1998 spectrum by a factor of 100 with respect to the 1997 spectrum.

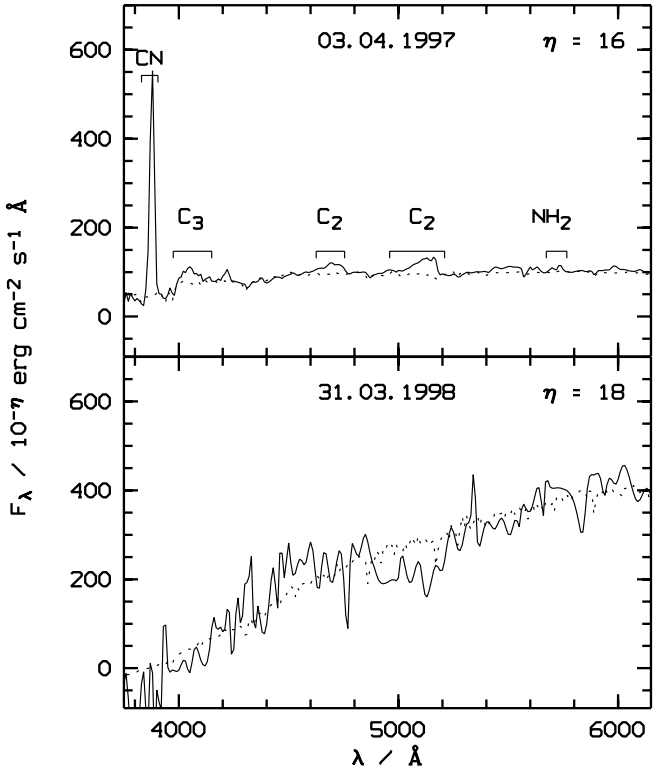

Fig. 6. Same as Fig. 5 only before continuum subtraction.

Table 6. $Af\rho$ values (aperture radius 10^4 km) obtained from broad band R images of Comet 81P/Wild 2.

Date	$Af\rho$
	cm
11.09.1996	206 ± 26
11.12.1996	347 ± 28
02.04.1997	507 ± 21
31.03.1998	406 ± 77

Table 7. Production rates, Q, and fluxes in Comet 81P/Wild 2.

Q	03.04.1997	31.03.1998
10^{24} s^{-1}		
$Q_{\rm CN}$	16.07 ± 0.33	<0.30
$Q_{\rm C_3}$	0.233 ± 0.008	<0.014
$Q_{\rm C_2}$	8.19 ± 0.19	<0.78
$Q_{\rm NH_2}$	8.36 ± 0.22	<0.40
$Af\rho$ (cm)	486 ± 26	407 ± 44
Flux*	03.04.1997	31.03.1998
10^{-16} erg cm^{-2} s^{-1}		
CN	12392	<19.8
C_3	3886	< 9.4
C_2	7857	<48.7
NH_2	627.9	<1.5
dust	21248	3220

Table 7 also lists the photometric fluxes measured in the 4″ by 2″slit, as production rates are strongly model-dependent. It is well known that the use of different models (Vectorial versus Haser Model in most cases) and different lifetimes/scalelengths leads to systematic, model dependent differences between the resulting production rates. We have compared our values of 3 April 1997 with those obtained for 2 April 1997 by Fink et al. (1999) who determined production rates of CN, C_2, and NH_2 from different emission bands (CN: 9100 Å, C_2: 5520 Å, NH_2: 6335 Å) and using the Haser model with considerably different scalelengths. Both data sets show large differences, particularly in the CN and the NH_2 production rate for which Fink et al. (1999) determined values that are higher by factors of ∼2.5, and ∼5, respectively. The obvious disagreement of the NH_2 production rate might be the due to

the fact that our NH_2 production rate was determined from the 0,10,0 emission, whereas Fink et al. (1999) used the 0,8,0 NH_2 emission for their production rate determination which is blended with the forbidden oxygen line at 6300 Å. In any case, it is evident that one has to be extremely careful when trying to classify comets according to their production rate ratios on the basis of just one set of data. Nevertheless, in spite of the large differences, both data sets confirm the depleted abundance of C_2 with regard to CN observed during previous apparitions (e.g. Osip et al. 1992; A'Hearn et al. 1995).

4. Summary and conclusions

The monitoring of the coma morphology of comet 81P/Wild 2 in three broad-band filters (B, V, R) revealed the presence of fan structures which were observable while the comet moved along its preperihelion orbit. The fans were clearly detected between heliocentric distances of $r = 2.1$ AU (Dec. 1996) to $r = 1.6$ AU (Apr. 1997), but are indicated already in a low signal-to-noise image obtained at $r = 2.6$ AU. The projected position of the fans appears to be rather stationary during that time period although the position angle of the Sun changed by about 180° between 1996 and 1997. No indication of distinct coma features was found in the only postperihelion observations taken $r = 3.2$ AU. However, as the comet was very far from the Sun, the signal-to-noise of these observations was too low to firmly conclude from non-detection on the non-presence of features. The fly-by of the Stardust spacecraft will take place at $r = 1.86$ AU postperihelion, which is about 5 months after the comet is at $r = 1.6$ AU preperihelion, the distance at which two fans were clearly detected during its 1997 apparition. Hence, it is not unlikely that the comet will exhibit similar structures at the time of the Stardust encounter.

The analysis of the radial distribution of the coma brightness and its evolution as a function of distance to the Sun showed no surprising results. The shape of the coma profiles is consistent with what is expected by the fountain model. The evolution of the dust production along the orbit seen in the $Af\rho$ values determined in broad-band R indicates that the postperihelion decrease of the dust production is shallower than the preperihelion increase. From the avaliable data, we estimate that the $Af\rho$ value at the time of the *Stardust* encounter should be close to the value at $r = 1.6$ AU preperihelion.

The compositional analysis of 81P/Wild 2 confirmed the depleted abundance of C_2 with regard to CN in this comet. The comparison of our production rates with those of Fink et al. (1999) demonstrated once again how crucial it is to critically review and discuss production rate values that were derived in different ways before drawing conclusions on trends or trying to classify a comet on the basis of production rate ratios.

Acknowledgements. We thank the European Southern Observatory for the allocation of observing time and the staff at ESO La Silla for their continuous support during the observations.

References

A'Hearn, M. F., Schleicher, D. G., Feldman, P. D., Millis, R. L., & Thompson, D. T. 1984, AJ, 89, 579
A'Hearn, M. F., Millis, R. L., Schleicher, D. G., Osip, D. J., & Birch, P. V. 1995, Icarus, 118, 223
Arpigny, C. 1995, ASP Conf. Ser., 81, 205
Bender, R., & Möllenhof, C. 1987, A&A, 177, 71
Bessell, M. S., Castelli, F., & Plez, B. 1998, A&A, 333, 231
Brewer, J., & Storm, J. 2001, Observing At The Danish 1.54 m Telescope: A Users Manual For The TCS And DFOSC, European Southern Observatory, LSO-MAN-ESO-22100-00002
Brownlee, D. E., Tsou, P., Clark, B. C., Swanson, P. N., & Vellinga, J. 1994, http://stardust.jpl.nasa.gov/science/sci2.html
Cochran, A. L., & Barker, E. 1986, ESA SP-250, Vol. I, 439
Colina, L., Bohlin, R. C., & Castelli, F. 1996, AJ, 112, 307
ESO-MIDAS User Guide, MIDAS Release 98NOV, European Southern Observatory, MID-MAN-ESO-11000-0002&3
Festou, M. C. 1981, A&A, 95, 69
Fink, U., Hicks, M. P., & Fevig, R. A. 1999, Icarus, 141, 331
Jewitt, D. C., & Meech, K. 1987, ApJ, 317, 992
Kawakita, H., Watanabe, J., Kinoshita, D., et al. 2001, PASJ, 53, L5
Kiehling, R. 1987, A&AS, 69, 465
Landolt, A. U. 1992, AJ, 104, 340
Marsden, B. G. 1978, IAU Circular, 3167
Melnick, J., & Mendes de Oliveira, C. 1995, EFOSC2 Operating Manual, European Southern Observatory, Garching, Germany
Osip, D. J., Schleicher, D. G., & Millis, R. L. 1992, Icarus, 98, 115
Patat, F. 1999, EFOSC2 User's Manual, European Southern Observatory, LSO-MAN-ESO-36100-0004
Schleicher, D. G. 1983, The Flouresence Of Cometary OH And CN, Ph.D. Thesis, Dept. Physics and Astronomy, University of Maryland, USA
Schulz, R. 1991, Proceedings 3rd ESO/ST-ECF Data Analysis Workshop, ed. P. J. Grosbol, & R. M. Warmels, 73
Schulz, R., McFadden, L. A., Chamberlin, A. B., A'Hearn, M. F., & Schleicher, D. G. 1994, Icarus, 109, 145
Schulz, R., Arpigny, C., Manfroid, J., et al. 1998, A&A, 335, L46
Sekanina, Z., in Diversity and Similarity of Comets, ed. E. J. Rolfe, & B. Battrick, ESA SP-278, 315
Sekanina, Z., & Boehnhardt, H. 1997, EMP 78, 313
Tegler, A., & Wyckoff, S. 1989, ApJ, 343, 445
Tüg, W. 1977, The Messenger (ESO) 11, 7